

The Novikov–Veselov equation and the inverse scattering method: II. Computation

This article has been downloaded from IOPscience. Please scroll down to see the full text article.

2012 Nonlinearity 25 1799

(<http://iopscience.iop.org/0951-7715/25/6/1799>)

View [the table of contents for this issue](#), or go to the [journal homepage](#) for more

Download details:

IP Address: 147.87.102.2

The article was downloaded on 22/05/2012 at 15:14

Please note that [terms and conditions apply](#).

The Novikov–Veselov equation and the inverse scattering method: II. Computation

M Lassas¹, J L Mueller², S Siltanen¹ and A Stahel³

¹ Department of Mathematics and Statistics, University of Helsinki, Finland

² Department of Mathematics and School of Biomedical Engineering, Colorado State University, Fort Collins, CO, USA

³ Department of Mathematics, Bern University of Applied Sciences, Engineering and Information Technology, Biel, Switzerland

E-mail: mueller@math.colostate.edu

Received 7 July 2011, in final form 11 April 2012

Published 18 May 2012

Online at stacks.iop.org/Non/25/1799

Recommended by A S Fokas

Abstract

The Novikov–Veselov (NV) equation is a $(2 + 1)$ -dimensional nonlinear evolution equation generalizing the $(1 + 1)$ -dimensional Korteweg–deVries equation. The inverse scattering method (ISM) is applied for numerical solution of the NV equation. It is the first time the ISM is used as a computational tool for computing evolutions of a $(2 + 1)$ -dimensional integrable system. In addition, a semi-implicit method is given for the numerical solution of the NV equation using finite differences in the spatial variables, Crank–Nicolson in time, and fast Fourier transforms for the auxiliary equation. Evolutions of initial data satisfying the hypotheses of part I of this paper are computed by the two methods and are observed to coincide with significant accuracy.

Mathematics Subject Classification: 47J35, 37K15

 Online supplementary data available from stacks.iop.org/Non/25/1799/mmedia

(Some figures may appear in colour only in the online journal)

1. Introduction

We present two new numerical solution methods for the nonlinear Novikov–Veselov (NV) equation

$$\frac{\partial q_\tau}{\partial \tau} = -\partial_z^3 q_\tau - \bar{\partial}_z^3 q_\tau + \frac{3}{4} \partial_z (q_\tau v_\tau) + \frac{3}{4} \bar{\partial}_z (q_\tau \bar{v}_\tau), \quad (1.1)$$

$$v_\tau(z) = \bar{\partial}_z^{-1} \partial_z q_\tau(z), \quad (1.2)$$

where $\tau \geq 0$ and $\bar{\partial}_z = \frac{1}{2}(\frac{\partial}{\partial x} + i\frac{\partial}{\partial y})$. Here $q_\tau(z) = q_\tau(x, y)$ is a real-valued function of variables $z = (x, y) \in \mathbb{R}^2$. The initial value $q_0(z)$ needs to be of a specific form described below, but

does not have to be small. Equation (1.1), introduced in [18, 26], is a (2+1)-dimensional generalization of the Kvd equation. One of our methods solves (1.1) directly using finite differences, and the other method is based on an inverse scattering transform.

The inverse scattering method (ISM) for the NV equation takes the following form:

$$\begin{array}{ccc}
 t_0(k) & \xrightarrow{\exp(i\tau(k^3 + \bar{k}^3))} & t_\tau(k) \\
 \uparrow \mathcal{T} & & \uparrow \mathcal{T} \\
 & & q_\tau^{\text{IS}}(z) \\
 \downarrow \mathcal{Q} & & \downarrow \mathcal{Q} \\
 q_0(z) & \xrightarrow{\text{nonlinear evolution (1.1)}} & q_\tau^{\text{NV}}(z).
 \end{array} \tag{1.3}$$

Here \mathcal{T} and \mathcal{Q} stand for the direct and inverse nonlinear Fourier transform, discussed in more detail in sections 2.2 and 2.4, respectively. The function $t_\tau : \mathbb{C} \rightarrow \mathbb{C}$ is called the *scattering transform*. We denote by $q_\tau^{\text{NV}}(z)$ the solution of equation (1.1) with initial data $q_0(z)$ and set

$$q_\tau^{\text{IS}}(z) = \mathcal{Q}\left(\exp(i\tau(k^3 + \bar{k}^3)) \mathcal{T}(q_0(\cdot))\right). \tag{1.4}$$

Now for certain initial data q_0 it holds that $q_\tau^{\text{IS}} \equiv q_\tau^{\text{NV}}$, see [19]. The diagram (1.3) is analogous to the celebrated ISM for the solution of the KdV equation introduced in [9].

The definition of the inverse nonlinear Fourier transform \mathcal{Q} is based on solving a D-bar equation. The D-bar methodology was developed by Beals and Coifman [4] within the framework of integrable nonlinear evolution equations in dimension (1+1) and was first applied to equations in dimension (2+1) in [1, 7]. By now it has been applied to many (2+1)-dimensional equations, see the reviews [5, 8], and thus the computational techniques introduced here have wide applicability.

It is shown in [14, 15] that the inverse scattering evolution q_τ^{IS} in (1.3) is well-defined, real-valued, and preserves conductivity type if the (possibly large) initial data q_0 are rotationally symmetric and of conductivity type. The term *conductivity type* is defined as follows.

Definition 1.1. A potential $q \in L^p(\mathbb{R}^2)$ with $1 < p < 2$ is of conductivity type if $q = \gamma^{-1/2} \Delta \gamma^{1/2}$ for some real-valued $\gamma \in L^\infty(\mathbb{R}^2)$ satisfying $\gamma(z) \geq c > 0$ for almost every $z \in \mathbb{R}^2$ and $\nabla(\gamma^{1/2}) \in L^p(\mathbb{R}^2)$.

The term ‘conductivity’ and the seemingly superficial square roots in definition 1.1 come from the related studies of Calderón’s inverse conductivity problem, see [17]. Furthermore, according to a recent result by Peter Perry [19], the equality $q_\tau^{\text{IS}} = q_\tau^{\text{NV}}$ holds in (1.3) for the choice of q_0 considered in part I of this paper [15].

This paper presents the first use of the ISM as a computational tool for computing evolutions of an integrable system in dimension (2 + 1). For the numerical use of the ISM for (1 + 1)-dimensional equations, see [20, 23]. Solving the NV equation by the ISM has certain advantages over the use of traditional approaches such as finite differences. First, one can compute the evolution at any desired time in a single computational step. Second, based on previous work we have proofs of convergence for the method used to solve the D-bar equation [12, 13] and estimates on the computational accuracy of the scattering transform [12]. The direct and inverse scattering algorithms used here were first developed in our research projects related to electrical impedance tomography.

We introduce also another algorithm, designed for direct computation of $q_\tau^{\text{NV}}(z)$. It is based on the numerical solution of the nonlinear partial differential equation (1.1) with auxiliary equation (1.2), performed using an implicit finite-difference method in the spatial variables, Crank–Nicolson in time, and fast Fourier transforms for the auxiliary equation.

Using the above two methods, we compute both q_τ^{IS} and q_τ^{NV} numerically for several initial potentials satisfying the assumptions of part I and find that the results agree with remarkable precision.

This paper is organized as follows. In section 2 we give some necessary background and describe the numerical implementation of the ISM. The direct numerical solution of equations (1.1) and (1.2) is described in section 3. A proof of the three-fold rotational invariance of solutions to the NV equation is given in section 4. Some conserved quantities in the NV evolution are derived in section 5. Numerical examples are provided in section 6.

2. Numerical solution by the ISM

2.1. Complex geometrical optics solutions

Assume that $q_0(z)$ is of conductivity type in the sense of definition 1.1. Consider the Schrödinger equation

$$(-\Delta + q_0)\psi(\cdot, k) = 0 \tag{2.1}$$

where $k \in \mathbb{C} \setminus 0$ is a parameter. Define the *complex geometrical optics* (CGO) solution ψ of equation (2.1) as the solution characterized by

$$e^{-ikz}\psi(z, k) - 1 \in L^{\tilde{p}} \cap L^\infty(\mathbb{R}^2) \quad \text{for fixed } k \in \mathbb{C} \setminus 0, \tag{2.2}$$

where $1 < p < 2$ and $1/\tilde{p} = 1/p - 1/2$. Here and throughout the paper a point $z = (x, y)$ in \mathbb{R}^2 (with a slight abuse of notation) will be identified with the complex number $z = x + iy \in \mathbb{C}$, so $\exp(ikz) = \exp(i(k_1 + ik_2)(x + iy))$.

As is shown in [17], ψ satisfies the Lippmann–Schwinger equation

$$\psi(z, k) = e^{ikz} - \int_{\mathbb{R}^2} G_k(z - \zeta)q_0(\zeta) d\zeta \tag{2.3}$$

where the function G_k is Faddeev’s Green’s function

$$G_k(z) := e^{ikz}g_k(z), \quad -\Delta G_k = \delta, \tag{2.4}$$

where g_k is given by

$$g_k(z) := \frac{1}{(2\pi)^2} \int_{\mathbb{R}^2} \frac{e^{iz \cdot \xi}}{|\xi|^2 + 2k(\xi_1 + i\xi_2)} d\xi, \quad (-\Delta - 4ik\bar{\partial}_z)g_k = \delta. \tag{2.5}$$

Note that the integral in (2.5) is not convergent and has to be interpreted in the sense of tempered distributions. An accurate numerical algorithm for $g_k(z)$ is described in [10, 21, 22].

Theoretical construction of the functions ψ is done via the functions $\mu(z, k) := e^{-ikz}\psi(z, k)$ by noting that μ satisfies for each fixed $k \in \mathbb{C} \setminus 0$

$$\mu = 1 - g_k * (q_0\mu). \tag{2.6}$$

Further, it is shown in [17] that $\mu(\cdot, k) - 1 \in W^{1, \tilde{p}}(\mathbb{R}^2)$ and that μ can be written as

$$\mu(\cdot, k) = 1 - [I + g_k * (q_0 \cdot)]^{-1}(g_k * q_0), \tag{2.7}$$

where the operator $I + g_k * (q_0 \cdot) : W^{1, \tilde{p}}(\mathbb{R}^2) \rightarrow W^{1, \tilde{p}}(\mathbb{R}^2)$ is invertible for any $k \in \mathbb{C} \setminus 0$.

2.1.1. The periodic formulation While formula (2.7) is constructive in the theoretical sense, numerical treatment calls for truncation of the computational domain.

We proceed by introducing a related periodic problem. Namely, assume that the initial potential $q_0(z)$ is supported in the unit disc. Take $\epsilon > 0$ and set $s = 2 + 3\epsilon$. Define a square $S := [-s, s]^2$ and choose a cutoff function

$$\eta \in C_0^\infty(\mathbb{R}^2), \quad \eta(x) = \begin{cases} 1 & \text{for } |x| < 2 + \epsilon, \\ 0 & \text{for } |x| > 2 + 2\epsilon. \end{cases} \quad (2.8)$$

Define a $2s$ -periodic approximate Green's function \tilde{g}_k almost everywhere by $\tilde{g}_k(z) := \eta(z)g_k(z)$ for all nonzero $z \in S$ and extending periodically:

$$\tilde{g}_k(z + j2s + i\ell 2s) = \eta(z)g_k(z) \quad \text{for } z \in S \setminus 0, \quad j, \ell \in \mathbb{Z}. \quad (2.9)$$

Also, extend q_0 periodically and call the result \tilde{q}_0 .

Now instead of the non-periodic equation (2.6) we consider the periodic equation

$$\tilde{\mu} = 1 - \tilde{g}_k \tilde{*} (\tilde{q}_0 \tilde{\mu}), \quad (2.10)$$

where $\tilde{*}$ denotes convolution on the torus. Analogously to (2.7) we can write

$$\tilde{\mu}(\cdot, k) = [I + \tilde{g}_k \tilde{*} (\tilde{q}_0 \cdot)]^{-1} 1, \quad (2.11)$$

where the existence of the inverse operator can be derived from the uniqueness of solution to (2.6).

Why would solving equation (2.10) be useful for the solution of (2.6)? It was shown in [3] that for any $k \in \mathbb{C} \setminus 0$ we have

$$\tilde{\mu}(z, k) = \mu(z, k) \quad \text{for } |z| < 1. \quad (2.12)$$

Combining (2.12), (2.6) and the fact that $\text{supp}(q_0) \subset D(0, 1)$ yields

$$\mu(z, k) = 1 - \int_{|\zeta| < 1} g_k(z - \zeta) q_0(\zeta) \tilde{\mu}(\zeta, k) \, d\zeta.$$

Thus the periodic solution of (2.10) gives the solution of (2.6) everywhere in the z -plane. The proof is a simplification of the proof of [3, theorem 2].

2.1.2. Approximate solution of the periodic equation Assume we are given a nonzero complex number k . Choose a positive integer m , denote $M = 2^m$, and set $h = 2s/M$. Define a grid $\mathcal{G}_m \subset Q$ by

$$\begin{aligned} \mathcal{G}_m &= \{jh \mid j \in \mathbb{Z}_m^2\}, \\ \mathbb{Z}_m^2 &= \{j = (j_1, j_2) \in \mathbb{Z}^2 \mid -2^{m-1} \leq j_\ell < 2^{m-1}, \ell = 1, 2\}. \end{aligned} \quad (2.13)$$

Note that the number of points in \mathcal{G}_m is M^2 . Define the grid approximation $\varphi_h : \mathbb{Z}_m^2 \rightarrow \mathbb{C}$ of a function $\varphi : Q \rightarrow \mathbb{C}$ by

$$\varphi_h(j) = \varphi(jh). \quad (2.14)$$

Our aim is to compute the matrix $\tilde{\mu}_h(j, k)$ approximately.

Recall the periodic Green's function \tilde{g} defined in (2.9), and set

$$\tilde{g}_h(j) = \begin{cases} \tilde{g}_k(jh), & \text{for } j \in \mathbb{Z}_m^2 \setminus 0, \\ 0, & \text{for } j = 0; \end{cases} \quad (2.15)$$

note that here the point $jh \in \mathbb{R}^2$ is interpreted as the complex number $hj_1 + ihj_2$. Now \tilde{g}_h is simply a $M \times M$ matrix with complex entries. Given a periodic function φ , the convolution $(\tilde{g}_k \tilde{*} \varphi)_h(j)$ is approximately given by

$$(\tilde{g}_k \tilde{*} \varphi)_h = h^2 f^{-1}(f(\tilde{g}_h) \cdot f(\varphi_h)), \quad (2.16)$$

where \mathcal{f} stands for discrete Fourier transform (DFT) and \cdot denotes element-wise matrix multiplication. This approach is based on the fact that convolution \star on the torus becomes multiplication under DFT. Note that the grid \mathcal{G}_m is defined so that fast Fourier transform is readily applicable to (2.16).

The final trick is to renumber the elements of any $M \times M$ matrix using just one index; in other words, to express functions given on grid points as vectors in $\mathbb{R}^{M \cdot M}$. Then equation (2.12) takes the form of a system of linear equations that can be solved using an iterative method, such as GMRES.

The numerical solution method discussed here was introduced by Vainikko [25] (see also [24]) for the Lippmann–Schwinger equation and later adapted to the present context in [16].

2.2. The nonlinear Fourier transform \mathcal{T}

The scattering transform $t_0 : \mathbb{C} \rightarrow \mathbb{C}$ of q_0 is defined by

$$t_0(k) = \int_{\mathbb{R}^2} e^{i\bar{k}z} q_0(x) \psi(z, k) \, dz, \tag{2.17}$$

where ψ is the CGO solutions to the Schrödinger equation (2.1) with asymptotics (2.2); here k is a nonzero complex parameter. We denote $\mathcal{T}q_0 = t_0$.

Why is \mathcal{T} called the nonlinear Fourier transform? This is because asymptotically $\psi(z, k) \sim e^{ikz}$ as $|z| \rightarrow \infty$, and substituting e^{ikz} in place of $\psi(z, k)$ into (2.17) results in

$$\begin{aligned} \int_{\mathbb{R}^2} e^{i(kz + \bar{k}\bar{z})} q_0(z) \, dx \, dy &= \int_{\mathbb{R}^2} e^{-i(-2k_1, 2k_2) \cdot (x, y)} q_0(z) \, dx \, dy \\ &= \widehat{q}_0(-2k_1, 2k_2). \end{aligned}$$

However, in (2.17) the function ψ depends on q_0 via the equation (2.1), and therefore the map $q_0 \mapsto \mathcal{T}q_0$ is nonlinear. The terminology dates back at least to 1974, as evidenced by the title of [2].

Formula (2.17) is not always well-defined. Given a general initial potential $q_0(\cdot) : \mathbb{R}^2 \rightarrow \mathbb{R}$, for some $k \in \mathbb{C} \setminus 0$ there may not exist a unique CGO solution of equation $(-\Delta + q_0)\psi(\cdot, k) = 0$ with the asymptotic property $\psi \sim e^{ikz}$ when z tends to infinity. Such k are called *exceptional points* of q . By [17] we know that potentials of conductivity type in the sense of definition 1.1 do not have exceptional points.

2.3. The D-bar equation

Given the initial scattering data $t_0(k)$, one can compute the scattering data of the evolved potential at time $\tau > 0$ simply by pointwise multiplication with the appropriate exponential function: $t_\tau(k) = \exp(i\tau(k^3 + \bar{k}^3))t_0(k)$. Determining the potential q_τ from the knowledge of t_τ is based on a so-called D-bar equation.

Denote $e_{-k}(z) = e^{-i(kz + \bar{k}\bar{z})}$. We look for functions μ_τ satisfying the D-bar equation

$$\bar{\partial}_k \mu_\tau(z, k) = \frac{t_0(k)}{4\pi\bar{k}} e_{-k}(z) \overline{\mu_\tau(z, k)}, \tag{2.18}$$

with the asymptotic condition

$$\mu_\tau(z, \cdot) - 1 \in L^\infty \cap L^r(\mathbb{C}) \quad \text{for fixed } z \in \mathbb{R}^2, \tag{2.19}$$

where $2 < r < \infty$.

Since $q_0(z)$ is of compactly supported and conductivity type, by [17, 14] the scattering transform $t_\tau(k)$ belongs to the Schwartz class, and the unique solution μ_τ to equation (2.18) can be determined as the unique solution of the integral equation

$$\mu_\tau(z, k) = 1 + \frac{1}{4\pi^2} \int_{\mathbb{R}^2} \frac{t_\tau(k')}{k'(k-k')} e_{-k'}(z) \overline{\mu_\tau(z, k')} dk. \quad (2.20)$$

In the numerical solution of (2.20), the integral is truncated to a set $\{|k| \leq R\}$ for some $R > 0$ generally chosen by inspection of the scattering transform, and a periodic formulation of (2.20) is utilized, defined in the same manner as section 2.1.1.

Note, however, that since the $\bar{\partial}$ equation (2.18) is only real-linear and not complex-linear due to the complex conjugate on the right-hand side of (2.18) and hence (2.20), one must write the real and imaginary parts of the unknown function μ_τ separately in the vector of function values at the grid points. (Another option would be to use a dedicated iterative method as described in [6].) It is proven in [12] that the error decreases as R tends to infinity. The truncated integral equation is solved numerically by the method described in [13] for each point z at which the evolved potential is to be computed.

2.4. The inverse nonlinear Fourier transform \mathcal{Q}

The inverse scattering map $\mathcal{Q} : t_\tau \mapsto q_\tau$ is defined by

$$(\mathcal{Q}t_\tau)(z) := \frac{i}{\pi^2} \bar{\partial}_z \int_{\mathbb{C}} \frac{t_\tau(k)}{k} e_{-k}(z) \overline{\mu_\tau(z, k)} dk, \quad (2.21)$$

where dk denotes Lebesgue measure on \mathbb{C} . The functions $\mu_\tau(z, k)$ in (2.21) are the unique solutions of the $\bar{\partial}$ equation (2.18) satisfying the asymptotics (2.19).

From [15, corollary 7.1], real-valued, smooth, rotationally symmetric initial data of compactly supported conductivity type remain of conductivity type under evolution by the ISM. Moreover, the evolved potential q_τ has no exceptional points. Thus, the conductivity γ_τ associated with the potential q_τ is given by

$$\gamma_\tau(z) = \mu_\tau(z, 0)^2. \quad (2.22)$$

Therefore, in the computations, q_τ is computed by numerical differentiation of γ_τ by the formula

$$q_\tau(z) = \gamma_\tau^{-1/2}(z) \Delta \gamma_\tau^{1/2}(z).$$

3. Numerical solution by the finite-difference method

To compare the ISM solution presented in section 2 we use a finite-difference approach, combined with a convolution argument. We chose not to use a spectral method for the problem, since the standard finite difference method allows for an easy implementation of the non-periodic boundary conditions. For periodic boundary conditions spectral methods are more efficient, see, for example, [11].

In this section we will suppress the subscript τ on q_τ and v_τ indicating the τ dependence in order to simplify the notation. Using the following identities, we rewrite the differential operator in (1.1) in a form more natural for finite-difference computations. We use

$$\begin{aligned} 4(\partial_z^3 + \bar{\partial}_z^3) &= \frac{1}{2} \left(\frac{\partial}{\partial x} - i \frac{\partial}{\partial y} \right)^3 + \frac{1}{2} \left(\frac{\partial}{\partial x} + i \frac{\partial}{\partial y} \right)^3 \\ &= \frac{\partial^3}{\partial x^3} - 3 \frac{\partial}{\partial x} \frac{\partial^2}{\partial y^2} \end{aligned}$$

and the nonlinear contribution in (1.1) can be written as follows:

$$\begin{aligned} 2 \partial_z (q v) &= 2 \partial_z ((q_1 + i q_2) (v_1 + i v_2)) \\ &= \left(\frac{\partial}{\partial x} (q_1 v_1 - q_2 v_2) + \frac{\partial}{\partial y} (q_1 v_2 + q_2 v_1) \right) \\ &\quad + i \left(\frac{\partial}{\partial x} (q_1 v_2 + q_2 v_1) - \frac{\partial}{\partial y} (q_1 v_1 - q_2 v_2) \right) \end{aligned}$$

and similarly for $2 \bar{\partial}_z (q \bar{v})$. This leads to

$$\begin{aligned} 2 \partial_z (q v) + 2 \bar{\partial}_z (q \bar{v}) &= 2 \left(\frac{\partial}{\partial x} (q_1 v_1) + \frac{\partial}{\partial y} (q_1 v_2) \right) \\ &\quad + i 2 \left(\frac{\partial}{\partial x} (q_2 v_1) + \frac{\partial}{\partial y} (q_2 v_2) \right) \end{aligned}$$

where $(v_1, v_2)^T$ is the solution of equation (1.2). Using $q = q_1 + i q_2$, $v = v_1 + i v_2$ and

$$\begin{aligned} 2 \partial_z q &= \left(\frac{\partial}{\partial x} q_1 + \frac{\partial}{\partial y} q_2 \right) + i \left(\frac{\partial}{\partial x} q_2 - \frac{\partial}{\partial y} q_1 \right) \\ 2 \bar{\partial}_z v &= \left(\frac{\partial}{\partial x} v_1 - \frac{\partial}{\partial y} v_2 \right) + i \left(\frac{\partial}{\partial x} v_2 + \frac{\partial}{\partial y} v_1 \right) \end{aligned}$$

the $\bar{\partial}$ equation (1.2) can be rewritten as a system of real equations.

$$\bar{\partial}_z v = \partial_z q \iff \begin{cases} \frac{\partial}{\partial x} v_1 - \frac{\partial}{\partial y} v_2 &= \frac{\partial}{\partial x} q_1 + \frac{\partial}{\partial y} q_2 \\ \frac{\partial}{\partial x} v_2 + \frac{\partial}{\partial y} v_1 &= \frac{\partial}{\partial x} q_2 - \frac{\partial}{\partial y} q_1. \end{cases}$$

If the initial value $q_0 = q_1 + i q_2$ is real valued ($q_2 = 0$) then all occurring expression remain real valued and we have to examine the nonlinear evolution equation

$$\frac{\partial}{\partial \tau} q = -\frac{1}{4} \frac{\partial^3}{\partial x^3} q + \frac{3}{4} \frac{\partial^3}{\partial x \partial y^2} q + \frac{3}{4} \operatorname{div} \left(q \begin{pmatrix} v_1 \\ v_2 \end{pmatrix} \right) \tag{3.1}$$

The three main challenges to consider for numerical solutions of the evolution equation by a finite-difference method are

- the linear contribution to the evolution equation: use a Crank–Nicolson scheme to preserve the L_2 norm,
- the $\bar{\partial}$ equation: use Green’s function and FFT to implement the convolution,
- the nonlinear contribution to the evolution equation: use an explicit scheme.

We consider each of these in turn in more detail.

3.1. The linear problem

The linear part of equation (3.1) is given by

$$\frac{\partial}{\partial \tau} q_\tau = -\frac{1}{4} \frac{\partial^3}{\partial x^3} q_\tau + \frac{3}{4} \frac{\partial^3}{\partial x \partial y^2} q_\tau = -A q_\tau \tag{3.2}$$

and we examine the domain $\Omega = [-L, L] \times [-L, L]$, i.e. $-L < x, y < L$. We have a known initial condition $q_0(x, y)$. Since we have an odd number of derivatives in the operator A we find by multiple integrations by parts

$$\langle u, A v \rangle = -\langle A u, v \rangle$$

Since the real $N^2 \times N^2$ matrix A is antisymmetric we examine the discrete conservation law using the midpoint \vec{m} between the points \vec{q}_i and \vec{q}_{i+1} and the directional vector \vec{w}

$$\begin{aligned} \vec{m} &= \frac{1}{2} (\vec{q}_{i+1} + \vec{q}_i) \\ \vec{w} &= \frac{1}{2} \Delta t (\vec{q}_{i+1} - \vec{q}_i) = -\frac{\Delta t}{4} A (\vec{q}_i + \vec{q}_{i+1}) = -\frac{\Delta t}{2} A \vec{m} \\ \langle \vec{m}, \vec{w} \rangle &= -\frac{\Delta t}{2} \langle \vec{m}, A \vec{m} \rangle = +\frac{\Delta t}{2} \langle A \vec{m}, \vec{m} \rangle = -\langle \vec{m}, \vec{w} \rangle \end{aligned}$$

and thus \vec{m} and \vec{w} are orthogonal. One CN step may be written as $\vec{q}_i = \vec{m} - \vec{w}$ and $\vec{q}_{i+1} = \vec{m} + \vec{w}$. Since

$$\begin{aligned} \|\vec{m} \pm \vec{w}\|^2 &= \langle \vec{m} \pm \vec{w}, \vec{m} \pm \vec{w} \rangle = \|\vec{m}\|^2 + \|\vec{w}\|^2 \pm \langle \vec{w}, \vec{m} \rangle \pm \langle \vec{m}, \vec{w} \rangle \\ &= \|\vec{m}\|^2 + \|\vec{w}\|^2 \end{aligned}$$

we conclude $\|\vec{q}_{i+1}\| = \|\vec{m} + \vec{w}\| = \|\vec{m} - \vec{w}\| = \|\vec{q}_i\|$ and we have a discrete conservation law. Based on the stability statement in the conservation law and the consistency of the finite-difference scheme we have convergence for the linear contribution.

Computational aspects and results. All matrices for the CN step are be created as sparse matrices. Since the same system of linear equations has to be solved for each step we perform an LU factorization first and then apply one back-substitution for each time step. For a mesh of the size $N \times N$ we work with

- matrices of the size $N^2 \times N^2$ with a semibandwidth of $2N$,
- LU factors L and U of the matrix $I + \frac{\Delta t}{2} A$ of size $N^2 \times N^2$ with full semibands of width $2N$, i.e. approximately $4N^3$ numbers to be stored in sparse matrices. This is the main memory need for this method,
- a computational effort for the LU factorization of $N^2 \times N^2$,
- a computational effort for each back-substitution of $2N^3$.

The above effects are confirmed by an implementation on a PC. Observe that storing one floating number in a sparse matrix requires a little more than one integer and one double to be stored, i.e. 12 byte. Thus we need approximately 770 MB of storage for a 256×256 grid.

3.2. Numerical solution of the $\bar{\partial}$ equation

To examine the $\bar{\partial}$ equation $\bar{\partial}_z v = f$ on the full plane, with the boundary condition $|v(z)| \rightarrow \infty$, we use Green’s function. Thus we determine a numerical solution of the $\bar{\partial}$ equation

$$\bar{\partial}_z v = f \quad \text{or} \quad \left(\frac{\partial}{\partial x} + i \frac{\partial}{\partial y} \right) v(x + iy) = 2 f(x + iy)$$

by

$$v(z) = \frac{1}{\pi} \iint_{\mathbb{R}^2} \frac{f(z')}{z - z'} dz'.$$

To compute this convolution integral we use a 2D-FFT. We have to restrict the computations on the square to be examined.

To be consistent with the finite-difference approximation of the linear part in equation (3.1) we examine a domain $[-L, L] \times [-L, L]$ with N interior nodes along each direction. We have (at first) N^2 nodes. Using FFT will quietly introduce a $2L$ periodicity and the convolution

kernel will pick up sizable contributions from neighbouring domains. Thus we enlarge the domain to twice the length in each direction and extend the function f by 0. We use the enlarged domain for the convolution kernel h . Consequently we perform the following steps.

- Discretize the function

$$h(z) = h(x, y) = \frac{1}{\pi (x + i y)}.$$

To avoid the singularity we choose a grid where the origin is not a node.

- Enlarge the domain to a larger domain, we use twice the side length. Use zero padding for the given function $f(x, y)$, but use the enlarged domain for h .
- Compute the 2D-FFT H as a complex matrix.
- Compute the 2D-FFT F of the given function $f(x, y)$.
- Compute $V = F \cdot H$ by pointwise multiplication and then $v = v_1 + i v_2$ as inverse 2D-FFT.
- Restrict the result on the smaller domain before returning the result.

3.3. A Semi-implicit method for the nonlinear problem

Denoting the nonlinear terms in equation (3.1) by M ,

$$M(q) = \frac{3}{4} \left(\frac{\partial}{\partial x} (q v_1) + \frac{\partial}{\partial y} (q v_2) \right), \quad (3.3)$$

we use the CN scheme for the linear part and an explicit method for the nonlinear part:

$$\begin{aligned} \frac{1}{\Delta t} (\bar{q}_{i+1} - \bar{q}_i) &= -\frac{1}{2} \mathbf{A} (\bar{q}_{i+1} + \bar{q}_i) + M(\bar{q}_i) \\ \left(\mathbb{I} + \frac{\Delta t}{2} \mathbf{A} \right) \bar{q}_{i+1} &= \left(\mathbb{I} - \frac{\Delta t}{2} \mathbf{A} \right) \bar{q}_i + \Delta t M(\bar{q}_i) \\ \bar{q}_{i+1} &= \left(\mathbb{I} + \frac{\Delta t}{2} \mathbf{A} \right)^{-1} \left(\left(\mathbb{I} - \frac{\Delta t}{2} \mathbf{A} \right) \bar{q}_i + \Delta t M(\bar{q}_i) \right). \end{aligned}$$

The computation of $M(q)$ is done in a sequence of steps.

- For a given function $q = q_\tau(x, y)$ compute

$$\partial_z q = \frac{1}{2} \left(\frac{\partial}{\partial x} q - i \frac{\partial}{\partial y} q \right)$$

using a finite-difference operator.

- Use the solution operator from section 3.2 to determine $v = v_1 + i v_2$ as solution of $\bar{\partial}_z v = \partial_z q$.
- Multiply the complex solution pointwise by q to obtain $q v$.
- Use a finite-difference operator to determine the desired expression $M(q)$ in (3.3).

All of the above computations have to be included in each CN step. There is no convergence proof yet for this scheme, but numerical experiments yield positive results.

4. Three-fold rotational symmetry

The NV equation has the special property of three-fold invariance. That is, assume that q is a solution of the evolution equation (1.1) and the initial condition $q_0(z)$ satisfies a three-fold rotational symmetry. Then for arbitrary times τ the solution $q_\tau(z)$ exhibits a three-fold symmetry.

To prove this result we have to verify that if $q_\tau(z)$ is invariant under rotations by $\phi = 120^\circ$, then $\frac{\partial q_\tau}{\partial \tau}$ is invariant. Let $R(x, y) = (x \cos \phi - y \sin \phi, x \sin \phi + y \cos \phi)$ represent a rotation by $\phi = 120^\circ$. We have to show that

$$q_\tau(R(x, y)) = q_\tau(x, y) \implies \frac{\partial}{\partial \tau} q_\tau(R(x, y)) = \frac{\partial}{\partial \tau} q_\tau(x, y).$$

It is convenient to examine the evolution equation in the form of equation (3.1) in our calculations. The three-fold invariance of q_0 implies

$$\frac{d^3}{dx^3} q_\tau(R(x, y)) = \frac{d^3}{dx^3} q_\tau(x, y) = \frac{\partial^3}{\partial x^3} q_\tau(x, y).$$

Using, for example, a symbolic calculation program one can verify

$$\left(-\frac{d^3}{dx^3} + 3 \frac{d^3}{dx dy^2} \right) q_\tau(R(x, y)) = \left(-\frac{\partial^3}{\partial x^3} + 3 \frac{\partial^3}{\partial x \partial y^2} \right) q_\tau(R(x, y)),$$

and thus if q_0 is a three-fold invariant we find

$$\left(-\frac{d^3}{dx^3} + 3 \frac{d^3}{dx dy^2} \right) q_\tau(R(x, y)) = \left(-\frac{\partial^3}{\partial x^3} + 3 \frac{\partial^3}{\partial x \partial y^2} \right) q_\tau(x, y).$$

This only holds for $\phi = \pm 120^\circ$ and is therefore the main reason for the three-fold symmetry. Thus, we see that the linear terms preserve the three-fold invariance. We will now see that the other contributions will not destroy this property. To consider the auxiliary equation in (1.1) $\bar{\partial}_z v_\tau = \partial_z q_\tau$, let $u(x, y) = v(x, y) + i w(x, y)$ and compute $2 \partial_z u = \left(\frac{\partial}{\partial x} - i \frac{\partial}{\partial y} \right) (v + i w) = v_x + w_y + i(-v_y + w_x)$, or using a vector notation

$$2 \partial_z \begin{pmatrix} v \\ w \end{pmatrix} = \begin{pmatrix} v_x + w_y \\ -v_y + w_x \end{pmatrix} \quad \text{and} \quad 2 \bar{\partial}_z \begin{pmatrix} v \\ w \end{pmatrix} = \begin{pmatrix} v_x - w_y \\ +v_y + w_x \end{pmatrix}.$$

By the chain rule

$$u_R(x, y) := u(R(x, y)) = u(x \cos \phi - y \sin \phi, x \sin \phi + y \cos \phi)$$

$$u_{R,x} = \frac{\partial}{\partial x} u_R(x, y) = u_x \cdot \cos \phi + u_y \cdot \sin \phi$$

$$u_{R,y} = \frac{\partial}{\partial y} u_R(x, y) = -u_x \cdot \sin \phi + u_y \cdot \cos \phi$$

and similarly for $v_{R,x}, v_{R,y}, w_{R,x}$ and $w_{R,y}$. Elementary algebra then leads to

$$2 \partial_z \begin{pmatrix} v_R \\ w_R \end{pmatrix} = \begin{pmatrix} v_{R,x} + w_{R,y} \\ -v_{R,y} + w_{R,x} \end{pmatrix} = \begin{bmatrix} +\cos \phi & -\sin \phi \\ +\sin \phi & +\cos \phi \end{bmatrix} \cdot 2 \partial_z \begin{pmatrix} v \\ w \end{pmatrix}$$

or, more concisely,

$$\partial_z u_R = \mathbf{R} \partial_z u. \tag{4.1}$$

Similar calculations show $\bar{\partial}_z u_R = \mathbf{R}^T \bar{\partial}_z u$. Now examine the $\bar{\partial}$ -equation

$$\bar{\partial}_z v = \partial_z q. \quad (4.2)$$

If $v(x, y)$ is a solution of (4.2) for a given $q(x, y)$ satisfying $q(R(x, y)) = q(x, y)$, then (4.1) implies

$$\partial_z q_R(x, y) = \mathbf{R} \partial_z q(R(x, y)) = \mathbf{R} \partial_z q(x, y).$$

Similarly,

$$\begin{aligned} \bar{\partial}_z v_R(x, y) &= \mathbf{R}^T \bar{\partial} v(R(x, y)) = \mathbf{R}^T \partial_z q_R(x, y) = \mathbf{R}^T \mathbf{R} \partial_z q(x, y) \\ &= \partial_z q(x, y), \end{aligned}$$

and consequently the rotated solution v_R solves the original problem. This implies that the solution v of (4.2) is rotationally invariant. It remains to verify that the expression $\operatorname{div}(q_\tau \vec{v}_\tau)$ in (3.1) is a three-fold invariant. The standard product rule and the assumptions $q_\tau(x, y) = q_\tau(R(x, y))$ and $\vec{v}_\tau(x, y) = \vec{v}_\tau(R(x, y))$ lead to the desired result.

5. Conserved quantities

To validate the numerical solution we use conserved quantities of the NV equations. The evolution is closely related to the KdV evolution, but the L_2 norm if the solution is not conserved. We consider using the two conserved expressions.

$$I_0 = \iint_{\mathbb{R}^2} q(z) \, dz \quad \text{and} \quad I_1 = \iint_{\mathbb{R}^2} q(z) (\bar{\partial}_z^{-1} q)(z) \, dz.$$

To verify that I_0 is constant, we use decaying conditions for all boundary contributions. Then integration leads to

$$\begin{aligned} \frac{d}{d\tau} I_0 &= \iint_{\mathbb{R}^2} \frac{d}{d\tau} q_\tau(z) \, dz \\ &= \iint_{\mathbb{R}^2} -\frac{1}{4} \frac{\partial^3}{\partial x^3} q_\tau + \frac{3}{4} \frac{\partial^3}{\partial x \partial y^2} q_\tau + \frac{3}{4} \operatorname{div} \left(q_\tau \begin{pmatrix} v_1 \\ v_2 \end{pmatrix} \right) \, dx \, dy = 0. \end{aligned}$$

For the numerical solution we cannot expect exact reproduction of I_0 , since there will be boundary contributions. Starting with a compact support we expect deviations to be very small at first and then get larger as time advances. We use an implicit scheme for the linear contributions, and consequently we will observe small deviations.

To examine the conserved quantity I_1 , let $w = \bar{\partial}_z^{-1} q$ and thus

$$\bar{\partial}_z w = q \quad \iff \quad \begin{cases} \frac{\partial}{\partial x} w_1 + \frac{\partial}{\partial y} w_2 = 2q_1 \\ \frac{\partial}{\partial x} w_2 - \frac{\partial}{\partial y} w_1 = 2q_2. \end{cases}$$

This leads to

$$\begin{aligned} I_1 &= \iint_{\mathbb{R}^2} q(z) (\bar{\partial}_z^{-1} q)(z) \, dz = \iint_{\mathbb{R}^2} q(z) w(z) \, dz \\ &= \iint_{\mathbb{R}^2} (q_1 + i q_2) (w_1 + i w_2) \, dz \end{aligned}$$

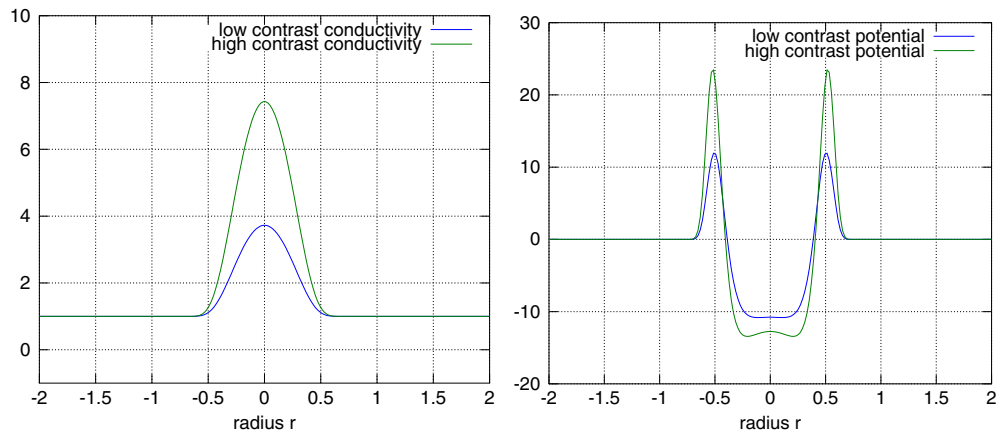


Figure 1. A cross-sectional plot of the low and high-contrast radially symmetric initial conductivities γ_0 (left) and potentials q_0 (right) in examples 1 and 2.

$$\begin{aligned}
 &= \frac{1}{2} \iint_{\mathbb{R}^2} \left(\left(\frac{\partial}{\partial x} w_1 + \frac{\partial}{\partial y} w_2 \right) + i \left(\frac{\partial}{\partial x} w_2 - \frac{\partial}{\partial y} w_1 \right) \right) (w_1 + i w_2) \, dz \\
 &= \frac{1}{2} \iint_{\mathbb{R}^2} \left(\frac{1}{2} \frac{\partial}{\partial x} (w_1^2) + \frac{\partial}{\partial y} (w_1 w_2) - \frac{1}{2} \frac{\partial}{\partial x} (w_2^2) \right) \, dz \\
 &\quad + \frac{i}{2} \iint_{\mathbb{R}^2} \left(\frac{\partial}{\partial x} (w_1 w_2) + \frac{1}{2} \frac{\partial}{\partial y} (w_2^2) - \frac{1}{2} \frac{\partial}{\partial y} (w_1^2) \right) \, dz = 0.
 \end{aligned}$$

Thus I_1 is independent of τ , without using the NV evolution. Based on this proof we do not use I_1 to validate the numerical solutions.

6. Numerical examples

The close agreement of the numerical solution of the evolution equation by the finite-difference method and the ISM is demonstrated on several examples. The examples are chosen such that $q_0(z)$ is radially symmetric to satisfy the assumptions of [15]. We also provide plots of the evolution of the potential for these examples. Animations of the time evolution are available at stacks.iop.org/Non/25/1799/mmedia.

6.1. Example conductivities

Examples 1 and 2. We consider a high and a low contrast initial potential that is a C^∞ function of conductivity type. By increasing the contrast of the conductivity γ we increase the contribution of the nonlinear terms in equation (3.1). Since the initial potentials are radially symmetric, they can be easily viewed as cross-sectional plots (see figure 1 for such plots of γ and q_0 .)

Fix $0 < \rho < 1$ and let $F_\rho \in C_0^\infty(\mathbb{R})$ for $-\rho \leq x \leq \rho$ be given by

$$F_\rho(x) := e^{-\frac{2(\rho^2+x^2)}{(x+\rho)^2(x-\rho)^2}}, \tag{6.1}$$

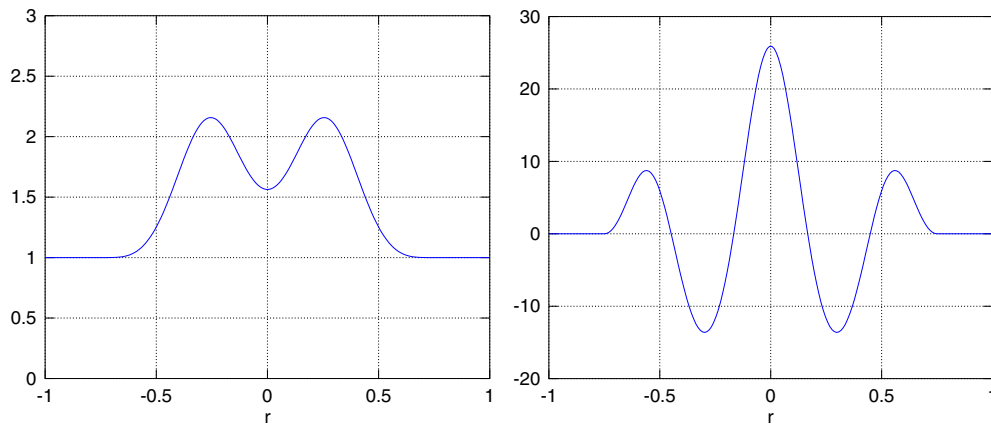


Figure 2. A cross-sectional plot of the radially symmetric initial conductivity γ_0 (left) and potential q_0 (right) for example 3.

and $F_\rho(x) = 0$ for $|x| > \rho$. We define γ by

$$\gamma(z) := \alpha F_\rho(|z|) + 1, \quad (6.2)$$

with $\rho = 0.95$, which results in a support of $B(0, \rho)$ for γ and q_0 . The Schrödinger potential q_0 is given outside the origin by

$$q_0(z) := \frac{\Delta \gamma^{1/2}(z)}{\gamma^{1/2}(z)} = \frac{\Delta F_\rho(|z|)}{F_\rho(|z|) + 1/\alpha}. \quad (6.3)$$

Note that $\gamma \equiv 1$ and $q \equiv 0$ for $|z| \geq \rho$. Choosing $\alpha = 25$ results in a maximum amplitude of approximately 12 for q_0 , which we will refer to as example 1. Choosing $\alpha = 59$ results in a maximum amplitude of approximately 24 for q_0 , which we will refer to as example 2. The nonlinear effects are only evident to the accuracy of our computations for the higher contrast example of $\alpha = 59$.

Example 3. The next example is a high amplitude C^2 function of conductivity type. As in the previous example, the contribution of the nonlinear terms increases as we increase the contrast in γ , and the initial potential is radially symmetric.

Define $F_\rho \in C_0^4(\mathbb{R})$ for $-\rho \leq x \leq \rho$ by

$$F_\rho(x) := (x^2 - \rho^2)^4 \left(1.5 - \cos \frac{3\pi x}{2\rho} \right), \quad (6.4)$$

and $F_\rho(x) = 0$ for $|x| > \rho$. Define γ by formula (6.2) with $\alpha = 5$ and $\rho = 3/4$ and q_0 by (6.3). Then $\max |q_0| \approx 26$. Plots of γ and the corresponding potential q_0 are found in figure 2.

6.2. Numerical evolutions

Contour plots of the real and imaginary parts of the evolution of the scattering transform $t_\tau(k)$ corresponding to example 1 are plotted for several τ in figure 3. Since the initial q_0 is radially symmetric and real, the initial scattering transform $t_0(k)$ is also radially symmetric and real. As τ increases, the imaginary part of t_τ grows. Also, the three-fold invariance in $t_\tau(k)$ is immediately visible in the plots. A movie of the evolving scattering transform both as a contour and three-dimensional plots is available at stacks.iop.org/Non/25/1799/mmedia.

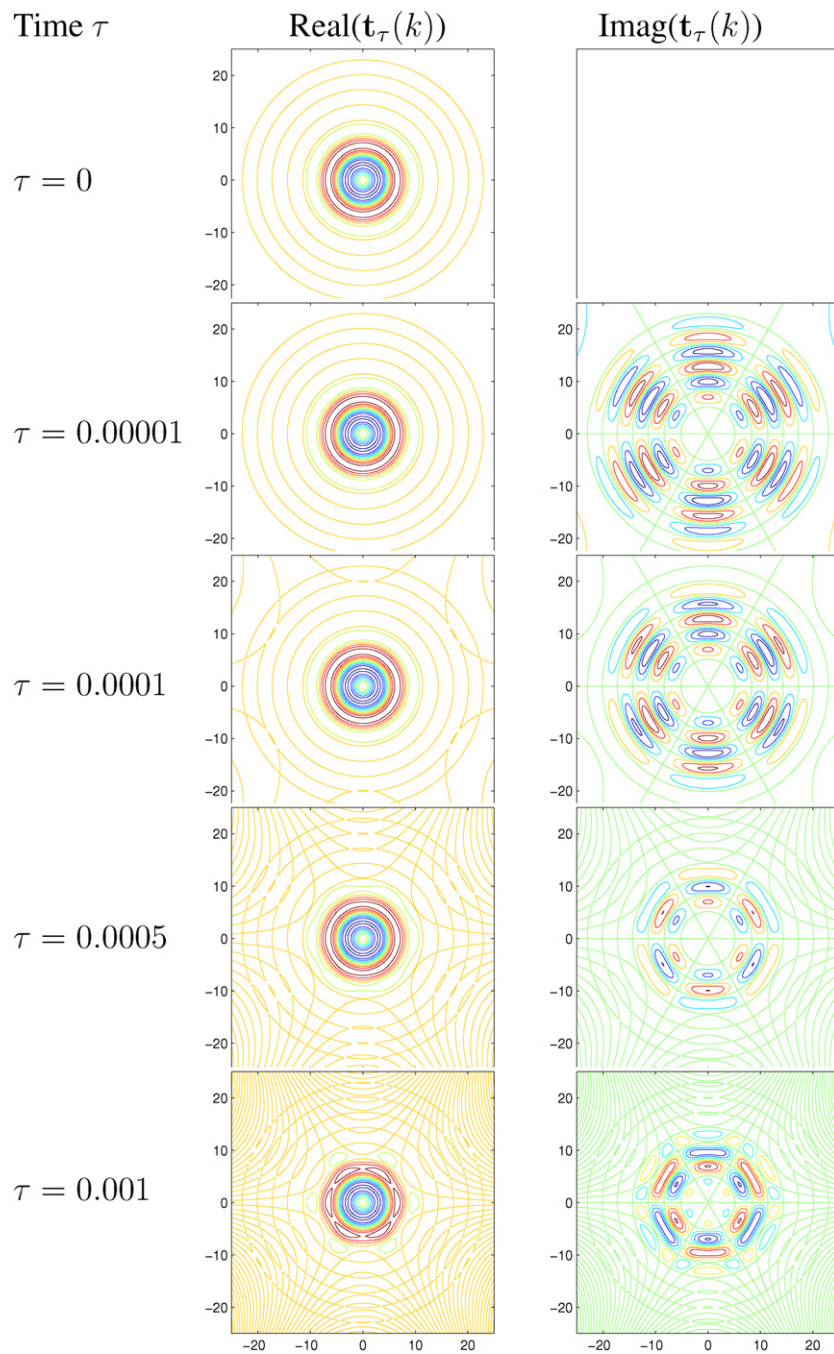


Figure 3. Contour plots of the real and imaginary parts of the evolving scattering transform $t_\tau(k)$ of example 1 for several values of τ . Since the initial q is radially symmetric and real, so is the initial scattering transform $t_0(k)$. As time evolves the imaginary part grows. Note the three-fold invariance in $t_\tau(k)$. Movies are available at stacks.iop.org/Non/25/1799/mmedia.

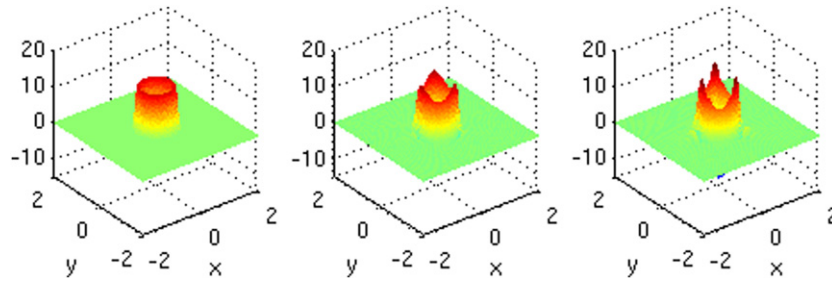


Figure 4. Time evolution of the solution q_τ at three times $t = 0, 3 \times 10^{-4}, 6 \times 10^{-4}$ for the low contrast example 1. A movie of the time evolution is available at stacks.iop.org/Non/25/1799/mmedia.

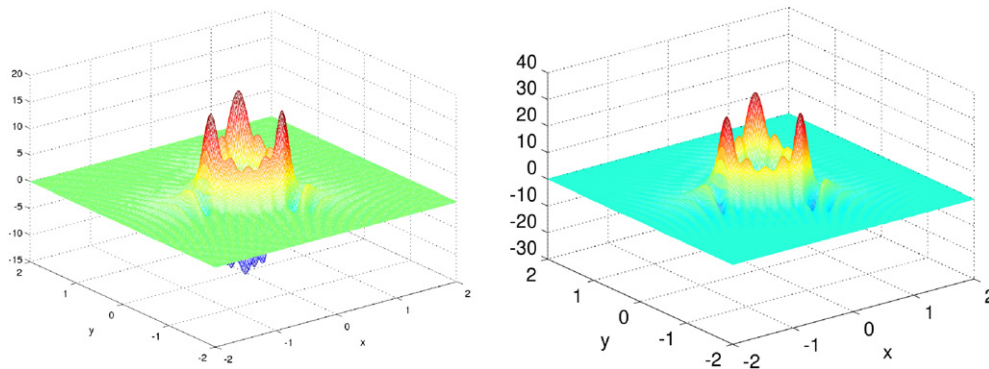


Figure 5. Time evolution of the solution q_τ at $\tau = 0.001$ for the low contrast example 1 (left) and the high contrast example 2 (right). A movie of the time evolution of each example is available at stacks.iop.org/Non/25/1799/mmedia.

Figure 4 shows the time evolution of example 1 at three times. Figure 5 shows the plots of both examples 1 and 2 at time 0.001 computed on a 512×512 grid. To illustrate the three-fold symmetry of the solution, we include a contour plot of example 2 in figure 6.

Concerning example 3, q_τ at $\tau = 0.001$ is shown in figure 7.

Time evolutions of all three solutions are given as movies available at stacks.iop.org/Non/25/1799/mmedia.

6.3. Discussion of accuracy

Let us start by noting that the solutions computed by the ISM and the finite-difference methods agree so closely that we only display in figures 4–7 the solution computed by the implicit finite-difference method. However, we performed a couple of additional accuracy tests as well and report the results below.

Denote the matrix representing the numerical approximation to q_τ computed by the ISM by q_τ^{IS} and the matrix representing the numerical approximation to q_τ computed by the implicit finite-difference method by q_τ^{FD} on the spatial grid defined above. The relative difference between the solutions at time τ is defined as

$$\text{RE} = \frac{\|q_\tau^{\text{IS}} - q_\tau^{\text{FD}}\|_\infty}{\|q_\tau^{\text{IS}}\|_\infty}.$$

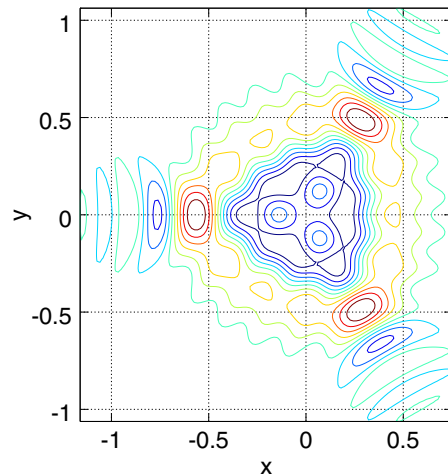


Figure 6. Contour plot of the solution q_τ at time $t = 0.001$ for the high contrast example 2.

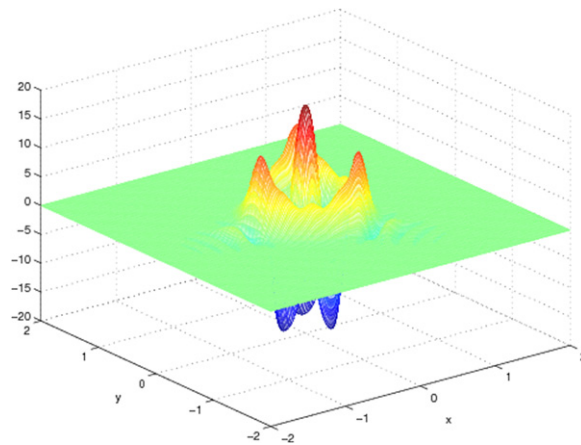


Figure 7. Time evolution of the solution q_τ at $\tau = 0.001$ for example 3. A movie of the time evolution is available at stacks.iop.org/Non/25/1799/mmedia.

In all computations, the relative error increased with τ . For both examples 1 and 2, it was only 10^{-3} at time $\tau = 0.001$. Figure 8 contains plots of the difference between the solutions computed by finite differences and the ISM for both the low amplitude example 1 and the high amplitude example 2. Figure 9 shows the difference between the ISM solution and the finite-difference solution for example 3. Very little structure is evident in the differences, indicating that the difference is likely due to the computational method rather than the underlying equation.

The agreement of the solution computed by the ISM and the implicit finite-difference scheme improves as we refine the grid. For the high contrast example, the mean absolute difference of the ISM solution and solution of the evolution equation drops from 0.12 to 0.04 as we move from a 256×256 grid to a 512×512 grid. For the low contrast example the mean differences drop from 0.044 to 0.038 for the 256×256 grid and the 512×512 grid, respectively.

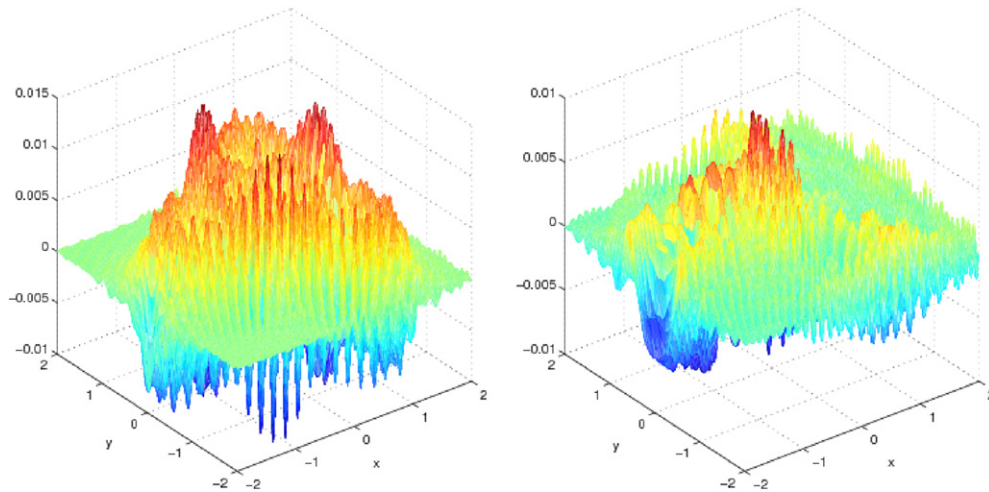


Figure 8. A plot of the difference between the solutions computed by finite differences and the ISM for the low contrast Example 1 (left) and the high contrast example 2. In each case, the relative error between the solutions is $\mathcal{O}(10^{-3})$ in L^∞ norm.

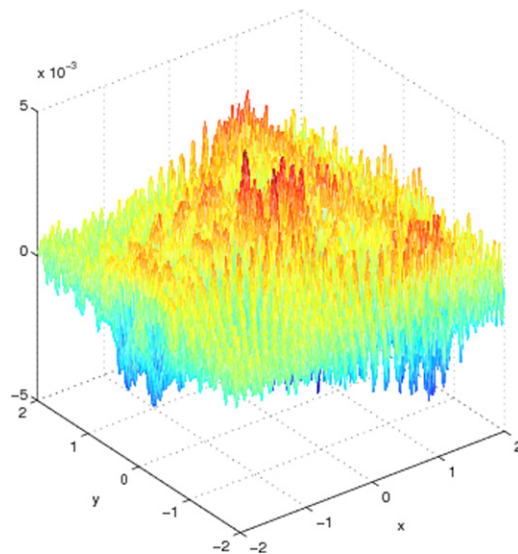


Figure 9. A plot of the difference between the solutions computed by finite differences and the ISM for example 3. The relative error between the solutions is $\mathcal{O}(10^{-3})$ in L^∞ norm.

The implicit finite-difference method is subject to errors due to reflections from the boundary and errors caused by the discretization of the partial derivatives.

Errors in the computation from the ISM arise from two main sources. One is the inevitable truncation of the scattering transform in the numerical solution of the D-bar equation (2.18), resulting in some smoothing of the reconstructed solution. These errors have been studied in the context of electrical impedance tomography in, for example, [12, 16]. The other source of error is the approximation performed in the solution of the periodic D-bar equation with truncated kernel. To study the latter error quantitatively, we computed the function $\mathcal{Q}(\tilde{t}_0)$ using

five different grids: 256×256 , 512×512 , 1024×1024 , 2048×2048 and 4096×4096 . Here $\tilde{t}_0(k) = t_0(k)$ for $|k| < 25$ and $\tilde{t}_0(k) = 0$ for $|k| \geq 25$. We measured the improvement of accuracy by comparing the results on the coarser grids to the result on the finest grid at several points $z \in \Omega$. The average relative sup norm errors were

$$\begin{array}{cccc} 256 \times 256 & 512 \times 512 & 1024 \times 1024 & 2048 \times 2048 \\ 0.105 & 0.027 & 0.006 & 0.001 \end{array} .$$

As discussed in section 5, the integral I_0 of the potential q_τ over the given square should be constant in τ . For example 1 we observe the value $I_0 = 2.0545$, with small variations between 2.0542 and 2.0551. For example 2 we find $I_0 = 5.295$, with small variations between 5.293 and 5.298. For both examples the variations increase as time advances. This is consistent with analytical reasoning.

References

- [1] Ablowitz M J, Bar Yaacov D and Fokas A S 1983 On the inverse scattering transform for the Kadomtsev–Petviashvili equation *Stud. Appl. Math.* **69** 135–143
- [2] Ablowitz M J, Kaup D J, Newell A C and Segur H 1974 The inverse scattering transform-Fourier analysis for nonlinear problems *Stud. Appl. Math.* **53** 249–315
- [3] Astala K, Mueller J L, Päiväranta L and Siltanen S 2010 Numerical computation of complex geometrical optics solutions to the conductivity equation *Appl. Comput. Harmonic Anal.* **29** 2–17
- [4] Beals R and Coifman R R 1981 Scattering, transformations spectrales et équations d'évolution non linéaires *Seminaire Goulaouic–Meyer–Schwartz 1980–1981* (Palaiseau: École Polytechnique)
- Beals R and Coifman R R 1982 Scattering, transformations spectrales et équations d'évolution non linéaires *Seminaire Goulaouic–Meyer–Schwartz 1981–1982* (Palaiseau: École Polytechnique) p 21
- [5] Beals R and Coifman R R 1986 The D-bar approach to inverse scattering and nonlinear evolution equations *Physica D* **18** 242–9
- [6] Eirola T, Huhtanen M and von Pfaler J 2003 Solution methods for \mathbb{R} -linear problems in \mathbb{C}^n *SIAM J. Matrix Anal. Appl.* **25** 804–28
- [7] Fokas A S and Ablowitz M J 1983 Method of solution for a class of multidimensional nonlinear evolution equations *Phys. Rev. Lett.* **51** 7–10
- [8] Fokas A S and Sung L-Y 1992 On the solvability of the N-wave, Davey–Stewartson and Kadomtsev–Petviashvili equations *Inverse Problems* **8** 673–708
- [9] Gardner C S, Greene J M, Kruskal M D and Miura R M 1967 Method for solving the Korteweg–deVries equation *Phys. Rev. Lett.* **19** 1095–7
- [10] Ikehata M and Siltanen S 2004 Numerical solution of the Cauchy problem for the stationary Schrödinger equation using Faddeev's Green function *SIAM J. Appl. Math.* **64** 1907–32
- [11] Klein C and Roidot K 2011 Fourth order time-stepping for Kadomtsev–Petviashvili and Davey–Stewartson equations arXiv:1108.3345v2 6
- [12] Knudsen K, Lassas M, Mueller J L and Siltanen S 2009 Regularized D-bar method for the inverse conductivity problem *Inverse Problems Imag.* **3** 599–624
- [13] Knudsen K, Mueller J L and Siltanen S 2004 Numerical solution method for the Dbar-equation in the plane *J. Comput. Phys.* **198** 500–17
- [14] Lassas M, Mueller J L and Siltanen S 2007 Mapping properties of the nonlinear Fourier transform in dimension two *Commun. PDEs* **32** 591–610
- [15] Lassas M, Mueller J L, Siltanen S and Stahel A 2011 The Novikov–Veselov equation and the inverse scattering method: I. Analysis *Physica D* at press (arXiv:1105.3903v1)
- [16] Mueller J L and Siltanen S 2003 Direct reconstructions of conductivities from boundary measurements *SIAM J. Sci. Comput.* **24** 1232–66
- [17] Nachman A I 1996 Global uniqueness for a two-dimensional inverse boundary value problem *Ann. Math.* **143** 71–96
- [18] Novikov S P and Veselov A P 1986 Two-dimensional Schrödinger operator: inverse scattering transform and evolutional equations *Physica D* **18** 267–73
- [19] Perry P 2012 Miura maps and inverse scattering for the Novikov–Veselov equation arXiv:1201.2385v1
- [20] Sacks Paul and Shin Jaemin 2009 Computational methods for some inverse scattering problems *Appl. Math. Comput.* **207** 111–23

-
- [21] Siltanen S 1999 Electrical impedance tomography and Faddeev Green's functions *Ann. Acad. Sci. Fenn. Math. Diss.* **121** 56
- [22] Siltanen S, Mueller J and Isaacson D 2000 An implementation of the reconstruction algorithm of A. Nachman for the 2-D inverse conductivity problem *Inverse Problems* **16** 681–99
Siltanen S, Mueller J and Isaacson D 2000 *Inverse Problems* **17** 1561–3 (erratum)
- [23] Trogdon T, Olver S and Deconinck B 2011 Numerical inverse scattering for the Kortewegde Vries and modied Kortewegde Vries equations *Technical Report 1397* The Mathematical Institute, University of Oxford, Eprints Archive
- [24] Vainikko G 1993 *Multidimensional Weakly Singular Integral Equations (Lecture notes in Mathematics vol 1549)* (Berlin: Springer) p 159
- [25] Vainikko G 2000 Fast solvers of the Lippmann–Schwinger equation *Direct and Inverse Problems of Mathematical Physics (Int. Soc. Anal. Appl. Comput. vol 5)* (Dordrecht: Kluwer Academic) p 423
- [26] Veselov A P and Novikov S P 1984 Finite-gap, two-dimensional potential Schrödinger operators. Explicit formulas and evolution equations *Dokl. Akad. Nauk. SSSR* **279** 20–4